

# CsMn<sub>4</sub>As<sub>3</sub>: A layered tetragonal transition-metal pnictide compound with antiferromagnetic ground state

Abhishek Pandey,<sup>\*,†,¶</sup> Saroj L. Samal,<sup>‡,§</sup> and David C. Johnston<sup>†</sup>

<sup>†</sup>*Ames Laboratory-USDOE and Department of Physics and Astronomy, Iowa State University, Ames, Iowa 50011, United States*

<sup>‡</sup>*Ames Laboratory-USDOE and Department of Chemistry, Iowa State University, Ames, Iowa 50011, United States*

<sup>¶</sup>*Current address: Department of Physics and Astronomy, Texas A&M University, College Station, Texas 77840, United States*

<sup>§</sup>*Current address: Department of Chemistry, National Institute of Technology, Rourkela, Odisha 769008, India*

E-mail: abhishek.phy@gmail.com

## Abstract

We report the synthesis and properties of a new layered tetragonal ternary compound CsMn<sub>4</sub>As<sub>3</sub> (structure: KCu<sub>4</sub>S<sub>3</sub>-type, space group:  $P4/mmm$ , No. 123 and  $Z = 2$ ). The material is a small band-gap semiconductor and exhibits an antiferromagnetic ground state associated with Mn spins. The compound exhibits a signature of a distinct magnetic moment canting event at 150(5) K with a canting angle of  $\approx 0.3^\circ$ . Although, some features of the magnetic characteristics of this new compound are qualitatively similar to those of the related BaMn<sub>2</sub>As<sub>2</sub>, the underlying Mn

sublattices of the two materials are quite different. While the Mn square-lattice layers in  $\text{BaMn}_2\text{As}_2$  are equally spaced along the  $c$ -direction with the interlayer distance  $d_{\text{L Ba}} = 6.7341(4)$  Å, the Mn sublattice forms bilayers in  $\text{CsMn}_4\text{As}_3$  with the interlayer distance within a bilayer  $d_{\text{L Cs}} = 3.1661(6)$  Å and the distance between the two adjacent bilayers  $d_{\text{B}} = 7.290(6)$  Å. This difference in the Mn sublattice is bound to significantly alter the energy balance between the  $J_1$ ,  $J_2$  and  $J_c$  exchange interactions within the  $J_1$ - $J_2$ - $J_c$  model compared to that in  $\text{BaMn}_2\text{As}_2$  and the other related 122 compounds including the well-known iron-arsenide superconductor parent compound  $\text{BaFe}_2\text{As}_2$ . Owing to the novelty of its transition metal sublattice, this new addition to the family of tetragonal materials related to the iron-based superconductors brings prospects for doping and pressure studies in the search of new superconducting phases as well as other exciting correlated-electron properties.

## Introduction

Discoveries of high- $T_c$  superconductivity in the layered cuprates<sup>1</sup> and 122-, 1111- and 111-type iron-based pnictides<sup>2</sup> suggest that the layered materials containing stacked square lattices of transition metal ions and with inherent antiferromagnetic (AFM) fluctuations/ordering are one of the most promising avenues for the search for new superconductors. After the surprising discovery of high- $T_c$  superconductivity in the iron-based compounds the search for new materials that may not necessarily contain iron but crystallize in the related layered structure began and as a result a few new superconductors were discovered.<sup>3</sup>  $\text{BaMn}_2\text{As}_2$ , which is isostructural to the well-known superconductor parent compound  $\text{BaFe}_2\text{As}_2$ , does not show superconductivity.<sup>4-6</sup> Instead, when doped with holes by replacing Ba with K or Rb,  $\text{BaMn}_2\text{As}_2$  exhibits half-metallic behavior and a novel magnetic ground state where local-moment AFM of the Mn-sublattice and itinerant ferromagnetism (FM) of the doped holes coexist with each other.<sup>7-13</sup> Intriguingly, the ordered-moment alignments in these two different types of collinear magnetic orders are orthogonal to each other. Whereas the moments

in the G-type AFM of Mn-spins are aligned along the tetragonal  $c$ -axis, the FM moments of the itinerant holes lie within the  $ab$ -plane.<sup>9,11</sup> Another consequence of the hole doping in  $\text{BaMn}_2\text{As}_2$  is a slow suppression of its Néel temperature  $T_N$  that is reduced from 625 K in the parent compound to 480 K in 40% hole-doped  $\text{Ba}_{0.6}\text{K}_{0.4}\text{Mn}_2\text{As}_2$ .<sup>8</sup> An extrapolation of the  $T_N$  versus doping concentration  $x$  suggests that full suppression of long-range AFM ordering might be achieved at  $x \approx 0.8$ .<sup>8</sup> Thus, by drawing an analogy with the iron-based counterpart  $\text{BaFe}_2\text{As}_2$ ,<sup>2</sup> one would anticipate the emergence of an interesting ground state in the fully ( $x = 1$ ) hole-doped  $\text{AMn}_2\text{As}_2$  compounds ( $A$ : alkali metal), where these hypothetical phases might be superconducting or at least serve as a potential parent compounds to new superconductors.

While our repeated attempts to synthesize the  $\text{AMn}_2\text{As}_2$  compounds failed for  $A = \text{Na}, \text{K}, \text{Rb}$  and  $\text{Cs}$ , in our endeavor we discovered a fascinating new tetragonal compound  $\text{CsMn}_4\text{As}_3$  which can be best described as a completely collapsed variant of the  $\text{BaMn}_2\text{As}_2$  where the entire middle layers of cations and As anions are absent, forming a  $\text{Mn}_4\text{As}_3$  bilayer of Mn atoms (Fig. 1). As a result, the ratio of the tetragonal lattice parameters  $c/a$  is only 2.44 in  $\text{CsMn}_4\text{As}_3$  compared to 3.23 in  $\text{BaMn}_2\text{As}_2$ .  $\text{CsMn}_4\text{As}_3$  is a small band-gap semiconductor that crystallizes in the  $\text{KCu}_4\text{S}_3$ -type structure<sup>14-16</sup> (space group  $P4/mmm$ ,  $Z = 2$ ). This structure is similar to those of the cuprates and the iron-based pnictides, containing a framework of stacked square lattices of transition metal (Mn) ions (Fig. 1). Additionally, our computational and experimental results indicate an AFM ground state in this material. Considering the stimulating observations made in the case of  $\text{BaMn}_2\text{As}_2$ , this new compound and its plausible variants appear to bring an opportunity to explore some new exciting electronic and/or magnetic ground states possibly including superconductivity.

## Experimental and Computational Details

**Synthesis.** Single crystals of  $\text{CsMn}_4\text{As}_3$  were grown by the solution growth technique using

MnAs self flux. Cs and MnAs were taken in a ratio of 1:4 in a 2 mL alumina crucible which was then sealed inside a Ta tube under  $\sim 1$  atm argon pressure. The Ta tube was then sealed inside a quartz tube under  $\sim 1/5$  atm argon pressure. The assembly was then heated to 1230 °C in about 20 h, kept there for 5 h and then cooled down to 1110 °C in 70 h. At this temperature the excess flux was decanted using a centrifuge. Several platelike shiny crystals of typical size  $5 \times 5 \times 0.5 \text{ mm}^3$  were obtained from the growth (Inset, Fig. 1S, supporting information).

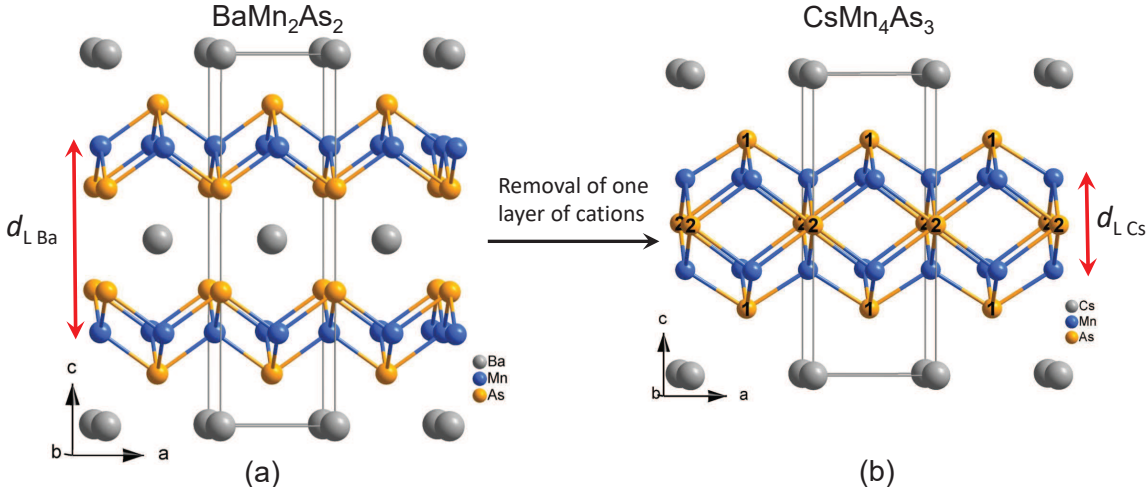


Figure 1: Crystal structures of tetragonal compounds (a)  $\text{BaMn}_2\text{As}_2$  and (b)  $\text{CsMn}_4\text{As}_3$ , where the latter is obtained by removing the middle layer of cations from the former. As1 and As2 atoms are indicated in (b) by numbers 1 and 2, respectively. The distance between the two adjacent Mn square-lattice layers are  $d_{L\text{Ba}} = c(1 - 2z_{\text{Mn}}) = 6.7341(4) \text{ \AA}$  in  $\text{BaMn}_2\text{As}_2$  and  $d_{L\text{Cs}} = c(1 - 2z_{\text{Mn}}) = 3.1661(6) \text{ \AA}$  in  $\text{CsMn}_4\text{As}_3$ .

**X-ray Diffraction Studies.** Powder x-ray diffraction (XRD) data were collected at room temperature using a Rigaku Geigerflex diffractometer utilizing  $\text{Cu-}K_\alpha$  radiation ( $\lambda = 1.54059 \text{ \AA}$ ). Rietveld refinement was performed using the FullPROF package<sup>17</sup> (Fig. S1, supporting information).

Single crystals of  $\text{CsMn}_4\text{As}_3$  were sealed in glass capillaries inside a  $\text{N}_2$ -filled glovebox. Single-crystal diffraction data sets were collected at room temperature over a  $2\theta$  range of  $\sim 6^\circ$  to  $\sim 60^\circ$  with  $0.5^\circ$  scans in  $\omega$  and 10 s per frame exposures with the aid of a Bruker SMART CCD diffractometer equipped with  $\text{Mo-}K_\alpha$  radiation ( $\lambda = 0.71073 \text{ \AA}$ ). The data

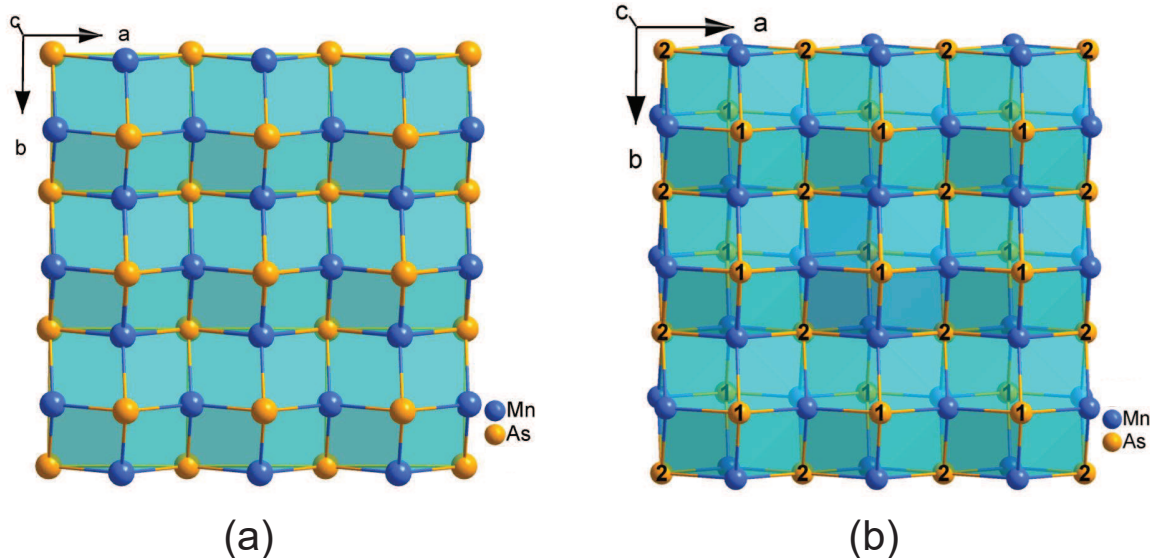


Figure 2: Arrangement of (a)  $[\text{Mn}_2\text{As}_2]^{-2}$  layer in  $\text{BaMn}_2\text{As}_2$  and (b)  $[\text{Mn}_4\text{As}_3]^{-1}$  bilayer in  $\text{CsMn}_4\text{As}_3$ . As1 and As2 atoms are indicated in (b) by numbers 1 and 2, respectively.

showed a primitive-tetragonal lattice and the intensity statistics indicated a centrosymmetric space group. The reflection intensities were integrated with the APEX II program in the SMART software package.<sup>18</sup> Empirical absorption corrections were employed using the SADABS program.<sup>19</sup> The space group  $P4/mmm$  (No. 123) of the structure was determined with the help of XPREP and SHELXTL 6.1.<sup>20</sup> The structure was solved by direct methods and subsequently refined on  $|F^2|$  with a combination of least-square refinements and difference Fourier maps.

The refinements of  $\text{CsMn}_4\text{As}_3$  converged to  $R_1 = 0.0709$ ,  $R_W = 0.0973$  for all data with goodness of fit 1.102 and maximum residuals of 3.92 and  $-1.68 \text{ e}/\text{\AA}^3$  that were 0.8 and 1.1  $\text{\AA}$  from the Cs and As2 sites, respectively. The refinement parameters and some crystallographic data are given in Table 1. The corresponding atomic positions and significant bond distances are listed in Table 2 and Table 4, respectively. The anisotropic displacement parameters are tabulated in Tables S1. The cif files are provided in the Supporting Information.

**Magnetic, Thermal and Electrical Transport Measurements.** Temperature  $T$ - and magnetic field  $H$ -dependent magnetic measurements were performed on an oriented

single crystal of CsMn<sub>4</sub>As<sub>3</sub> using a Quantum Design, Inc. (QDI), superconducting quantum interference device magnetometer. Heat capacity  $C_p$  versus  $T$  measurements were performed on a single crystal sample employing QDI's physical properties measurement system (PPMS) in two parts—first between 1.8 to 300 K using the N-grease and then between 290 to 344 K on the same crystal using the H-grease, where both N- and H-grease were supplied by QDI. In-plane electrical resistivity  $\rho_{ab}$  versus  $T$  measurements were performed on a single crystal sample using the PPMS over the  $T$  range of 1.8-300 K.

**Electronic Structure Calculations.** Electronic structure calculations on CsMn<sub>4</sub>As<sub>3</sub> were performed self-consistently using the tight-binding linear-muffin-tin-orbital (TB-LMTO) method within the atomic sphere approximation.<sup>21</sup> The simplest model that allows the AFM coupling was employed, which is in space group  $P4mm$  with two independent Mn atoms. The exchange and correlation were treated in the local spin-density approximation (LSDA) calculations. Scalar relativistic corrections were included.<sup>22</sup> The Wigner-Seitz radii of the spheres were assigned automatically so that the overlapping potentials would be the best possible approximation to the full potential.<sup>23</sup> The radii (Å) were: Cs = 2.39, Mn1 = Mn2 = 1.38, As1 = 1.61, As2 = As3 = 1.48. No additional empty spheres were needed subject to an 18% overlap restriction between atom-centered spheres. Basis sets of Cs  $6s, (6p, 5d, 4f)$ ; Mn  $4s, 4p, 3d$ ; and As  $4s, 4p, (4d)$  (downfolded orbitals in parentheses) were employed, and the tetrahedron method using a  $18 \times 18 \times 6$  mesh of  $k$ -points was applied to perform the reciprocal space integrations.

For bonding analysis, the crystal orbital Hamilton populations (COHPs)<sup>24</sup> of all filled electronic states for selected atom pairs were calculated. The weighted integration of COHP curves of these atom pairs up to the Fermi energy ( $E_F$ ) provides ICOHP values, i.e., total (integrated) Hamilton populations (Table 4), which are approximations of relative bond strengths. The COHP analyses provide the contributions of the covalent parts of particular pair-wise interactions to the total bonding energy of the crystal.

# Results and Discussion

**Structure.** A new layered tetragonal compound  $\text{CsMn}_4\text{As}_3$  has been discovered which crystallizes in the primitive-tetragonal space group  $P4/mmm$  (No. 123 and  $Z = 2$ ) and has a framework of  $[\text{Mn}_4\text{As}_3]^-$  layers and Cs-spacer atoms between the layers.  $\text{CsMn}_4\text{As}_3$  can be considered as a derivative of the well-known G-type AFM compound  $\text{BaMn}_2\text{As}_2$  ( $\equiv \text{Ba}_2\text{Mn}_4\text{As}_4$ ) that contains two layers of  $[\text{Mn}_2\text{As}_2]^{-2}$  with a cation spacer layer in between. When replacing Ba with Cs, one layer of cations is entirely removed and the two anion layers collapse to form a single  $[\text{Mn}_4\text{As}_3]^-$  layer in the resultant 143-compound  $\text{CsMn}_4\text{As}_3$  (Fig. 1). As a result, the  $c$ -axis is compressed to about 3/4 of the  $c$ -axis of  $\text{BaMn}_2\text{As}_2$ . This altered structure seems to primarily result from two synergetic effects—(i) charge balance between the cations and the anion, where the formal charge on  $\text{CsMn}_4\text{As}_3$  can be assigned according to the Zintl-Klemm rule by assuming complete electron transfer from cations to anions, yielding  $(\text{Cs}^+)[(\text{Mn}^{+2})_4(\text{As}^{-3})_3]$ ; and (ii) a weaker cation-anion interaction in  $\text{CsMn}_4\text{As}_3$  compared to that in the related compound  $\text{BaMn}_2\text{As}_2$ <sup>25</sup> as discussed in the "Electronic Structure and Chemical Bonding section" below.

The basic building block in the  $\text{CsMn}_4\text{As}_3$  structure is the  $\text{Mn}_8$  rectangular polyhedron in which all the faces are capped by As atoms leading into a  $\text{Mn}_8@As_6$  unit. This arrangement results as a consequence of the collapse of the two  $[\text{Mn}_2\text{As}_2]^{-2}$  layers into a single  $[\text{Mn}_4\text{As}_3]^-$  layer. The face-capped  $\text{Mn}_8@As_6$  polyhedra are connected through Mn–Mn and Mn–As bonds. In contrast, the basic building units in the  $\text{BaMn}_2\text{As}_2$  structure are the square networks of Mn atoms capped by As atoms. These  $\text{Mn}_4$  blocks are edge-shared in the  $ab$ -plane to form a 2D layer with each  $\text{Mn}_4$  square capped by an As atom in a zigzag manner (Fig. 2).

There are two types of arsenic atoms present in  $\text{CsMn}_4\text{As}_3$ —the bridging As atoms (As1) that are bonded to eight Mn atoms in a rectangular geometry and the terminal As atoms (As2) that are bonded to four Mn atoms in a similar way as in  $\text{BaMn}_2\text{As}_2$  which has only one type of As atom (Fig. 1). In  $\text{CsMn}_4\text{As}_3$ , each Mn is bonded to four As in a distorted

Table 1: Crystal data and the structural refinement parameters for CsMn<sub>4</sub>As<sub>3</sub> that crystallizes in a tetragonal structure with  $P4/mmm$  (No. 123) space group symmetry and  $Z = 2$  formula units/cell.

Parameter	Estimated value/range
Formula weight (g)	577.42
Unit cell dimensions (Å)	$a = 4.2882(2)$ and $c = 10.456(2)$
Volume (Å <sup>3</sup> )	192.3(1)
Density (g/cm <sup>3</sup> )	4.98
Absorption coefficient (mm <sup>-1</sup> )	132.63
Theta range (degree)	1.98 to 28.998
Index ranges	$-4 \leq h \leq 5$ ; $-4 \leq k \leq 5$ ; $13 \leq l \leq 13$
Reflections collected	1725
Independent reflections	194
Data/parameters	194/12
Goodness-of-fit on $F^2$	1.102
Final $R$ indices [ $I > 2\sigma(I)$ ] <sup>a</sup>	$R_1 = 0.0593$ ; $wR_2 = 0.0865$
$R$ indices (all data)	$R_1 = 0.0709$ ; $wR_2 = 0.0973$
Largest diff. peak and hole (e Å <sup>-3</sup> )	3.92 [0.81 Å from Cs] and -1.68 [1.16 Å from As2]

<sup>a</sup> $R = \Sigma||F_o| - |F_c||/\Sigma|F_o|$ ;  $R_w = [\Sigma w(|F_o| - |F_c|)^2/\Sigma w(F_o)^2]^{1/2}$ ;  $w = 1/\sigma F^2$ .

tetrahedron geometry (Fig. S2, supporting information) with a longer bond length (2.666 Å) between Mn and shared As (As1) along the  $c$ -direction and a shorter bond length (2.533 Å) between Mn and the terminal As (As2). The As-Mn-As bond angle ranges from 107.08(1)° to 115.65(1)°, significantly deviating from an ideal tetrahedral geometry. On the other hand, in the case of BaMn<sub>2</sub>As<sub>2</sub>, each Mn is bonded to four As in a slightly distorted tetrahedron (As-Mn-As bond angle 108.64° – 109.89°) with equal Mn–As bond distances (2.566 Å).<sup>2</sup>

Table 2: Wyckoff positions, site point symmetry, atomic coordinates and isotropic equivalent displacement parameters for CsMn<sub>4</sub>As<sub>3</sub>.

atom	Wyckoff	site	$x$	$y$	$z$	$U_{eq}(\text{Å}^2)$ <sup>a</sup>
Cs	1b	4/ $mmm$	0	0	0	0.023(1)
Mn	4i	2 $mm$	0	1/2	0.3486(2)	0.019(1)
As1	1a	4/ $mmm$	0	0	1/2	0.022(1)
As2	2h	4 $mm$	1/2	1/2	0.2202(2)	0.012(1)

<sup>a</sup> $U_{eq}$  is defined as one-third of the trace of the orthogonalized  $U^{ij}$  tensor.

In the related iron-based analogue 143-compound CaFe<sub>4</sub>As<sub>3</sub> that crystallizes in an orthorhombic structure (space group:  $Pnma$ ), Fe atoms are in two different coordination

Table 3: Structural features and parameters, Pauling’s metallic radii  $r_{A(12)}$ ,  $A$ –As distance  $d_{A-As}$  ( $A = \text{Ba}, \text{Cs}$  and  $\text{Ca}$ ), Mn/Fe–As distances  $d_{\text{Mn/Fe-As}}$  and Néel temperature  $T_{\text{N}}$  for  $\text{BaMn}_2\text{As}_2$ ,  $\text{CsMn}_4\text{As}_3$  and  $\text{CaFe}_4\text{As}_3$ .

	$\text{BaMn}_2\text{As}_2$	$\text{CsMn}_4\text{As}_3$	$\text{CaFe}_4\text{As}_3$
Structure & Space group	Tetragonal, $I4/mmm$	Tetragonal, $P4/mmm$	Orthorhombic, $Pnma$
Structural Features	Layered structure that contains $[\text{Mn}_2\text{As}_2]^{-2}$ layers with cation layer as spacer.  Ba has cubic coordination by As.	Layered structure that contains $[\text{Mn}_4\text{As}_3]^{-1}$ layers with cation layer as spacer.  Cs has cubic coordination by As.	3D channel/tunnel like structure where cations fill the channel made of Fe and As.  Ca has trigonal prismatic coordination
Unit cell dimensions ( $\text{\AA}$ )	$a = 4.1684(2)$ $c = 13.4681(8)$ $c/a = 3.2309(4)$	$a = 4.2882(2)$ $c = 10.456(2)$ $c/a = 2.4383(6)$	$a = 11.918(2)$ $b = 3.749(1)$ $c = 11.625(3)$ $a/b = 3.179(1)$ $c/b = 3.101(2)$
$z_{\text{Mn}}$	1/2	0.3486(2)	–
$r_{A(12)}$ ( $\text{\AA}$ )	2.215	2.67	1.97
$d_{A-As}$ ( $\text{\AA}$ )	3.492	3.803	2.969-3.152
$d_{\text{Mn/Fe-As}}$ ( $\text{\AA}$ )	2.566	2.533 and 2.666	2.380-2.465 (CN = 4), 2.427-2.610 (CN = 5)
$T_{\text{N}}$ (K)	625	> 300	90 ( $T_{\text{N1}}$ ) and 26 ( $T_{\text{N2}}$ )

environments—a strongly distorted tetrahedron and a square pyramid, corresponding to two different sets of Fe–As bond lengths.<sup>26</sup> The compound has a 3D open framework containing a covalent channel consisting of Fe and As. The  $\text{Ca}^{+2}$  cations fill the channel that runs along the  $b$ -axis of the orthorhombic cell. Thus, although  $\text{CsMn}_4\text{As}_3$  and  $\text{CaFe}_4\text{As}_3$  have the same stoichiometry, they are structurally entirely different and their properties cannot be compared on the same footing (Table 3).

**Electronic Structure and Chemical Bonding.** Figures 3(a-d) show the total electronic density of states (DOS) along with the individual atom and orbital projections of the DOS for  $\text{CsMn}_4\text{As}_3$  obtained from the tight-binding LMTO calculations using the LSDA (both majority and minority spin states are combined within the diagrams). The calculations were carried out for an A-type collinear AFM model where the Mn spins are aligned along the  $c$ -axis within the space group  $P4mm$  (Fig. S3, supporting information). The COHP curves for each pair-wise interaction as a function of energy are shown in Fig. 3(e). The  $E_F$  lies in a nonzero DOS region of  $\mathcal{D}^{\text{band}}(E_F) \sim 5$  states/eV f.u. for both spin directions. This suggests a metallic character of the compound. The As 4s states lie below  $-11$  eV and are not shown in the DOS plot. The As 4p states appear mostly in the  $-5.2$  to  $2.0$  eV range. The Mn 3d states are spin polarized with a zero-temperature ordered magnetic moment of  $3.50 \mu_B$  per Mn atom. This value of the magnetic moment of Mn occurs because the majority spin states are nearly filled ( $4.5 e^-/\text{Mn}$ ) and the minority spin states are partially filled ( $1.0 e^-/\text{Mn}$ ) [Fig. 3(c)].

Chemical bonding features can be judged to some extent from the DOS and COHP curves as well as the integrated crystal orbital Hamilton population (ICOHP) data. The important bond distances and the average  $-ICOHP$  values for each bond type and their percent contributions to the total polar-covalent bonding per unit cell are listed in Table 4. The individual heteroatomic Mn–As orbital interactions have  $-ICOHP$  values of  $2.44$  eV and  $1.59$  eV for Mn–As2 and Mn–As1, respectively, which are significantly larger than all other contacts (Table 4). The bonding contributions of Mn–As and Mn–Mn contacts are 85%

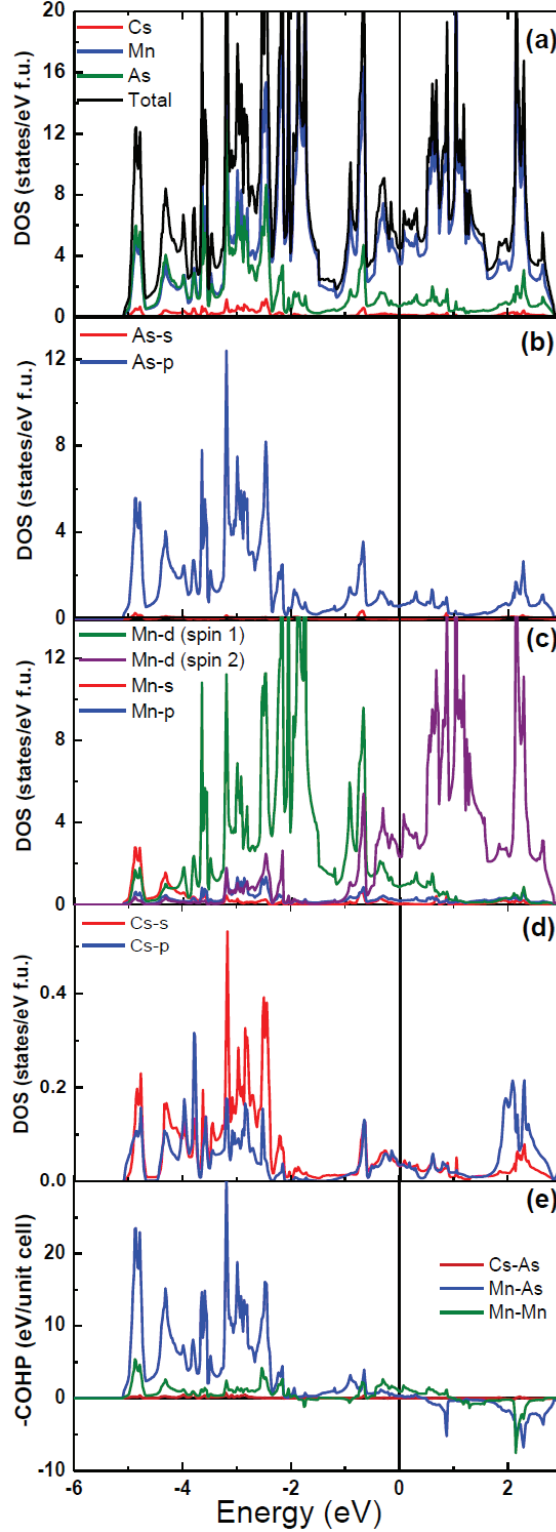


Figure 3: Results of spin-polarized LMTO-ASA calculations for  $\text{CsMn}_4\text{As}_3$ . (a) Total and atom decomposed densities of states (DOS). Partial projections of orbital DOS are shown for (b) As  $4s$  and  $4p$ ; (c) Mn  $4s$ ,  $4p$  and spin-polarized  $3d$  (d) Cs  $6s$  and  $6p$ . (e) COHP values for Cs–As, Mn–As and Mn–Mn. The DOS's plotted in figures (a) to (d) are for both spin directions. In all five panels the Fermi energy is set to zero.

Table 4: Bond lengths, average molar integrated crystal orbital Hamilton population (ICOHP) values, number of bonds per cell  $n$  and percentage contribution of each type of bond to the total bonding per unit cell for  $\text{CsMn}_4\text{As}_3$  obtained from the spin polarized calculations.

Bond	Length(Å)	-ICOHP/bond(eV)	$n$	-ICOHP/cell	%
Mn1-As1	2.533(1)	2.44	4	9.76	25.9
Mn2-As2	2.533(1)	2.44	4	9.76	25.9
Mn1-As3	2.665(1)	1.59	4	6.36	16.9
Mn2-As3	2.665(1)	1.59	4	6.36	16.9
Mn1-Mn1	3.032(2)	0.55	4	2.2	5.8
Mn2-Mn2	3.032(2)	0.55	4	2.2	5.8
Mn1-Mn2	3.170(2)	0.27	2	0.54	1.4
Cs-As	3.802(2)	0.07	8	0.56	1.5

and 13%, respectively, making them the most dominant contributors to the total bonding energy. The -ICOHP value of individual polar heteroatomic Cs-As orbital interactions is 0.07 eV, which contributes only about 2% to the total bonding energy. This indicates a very weak Cs-As interaction in  $\text{CsMn}_4\text{As}_3$ , which is likely one of the reasons for the absence of the intermediate cation layer in this compound. A similar weak cation-anion interaction was observed in  $\text{Na}_6\text{Au}_7\text{Cd}_{16}$ ,<sup>27</sup> which is closely related to  $\text{Ca}_6\text{Pt}_8\text{Cd}_{16}$ .<sup>25</sup> In the latter compound a strong cation-anion (Ca-Pt) bonding was observed due to the availability of  $3d$  orbitals of Ca which are naturally lacking in Na. To compare the bond energies of the  $A$ -As ( $A = \text{Ba}$  or  $\text{Cs}$ ) bonds in the presently reported and the  $\text{BaMn}_2\text{As}_2$  structure types, we have performed calculations on  $\text{Cs}T_4\text{As}_3$  ( $T = \text{Mn}, \text{Zn}$  and  $\text{Cd}$ ) and  $\text{BaMn}_2\text{As}_2$  compounds (Table S2, supporting information). The calculations show that the -ICOHP value for the Ba-As bond is double than that of the Cs-As bonds, which indicates a weaker cation-anion interaction in  $\text{Cs}T_4\text{As}_3$  compared to that in the  $\text{BaMn}_2\text{As}_2$ . In addition, the number of such bonds per unit cell in  $\text{BaMn}_2\text{As}_2$  are double the number of those bonds in  $\text{CsMn}_4\text{As}_3$ . Hence the bond energy contribution of the  $A$ -As interaction per unit cell toward the structure stability in the later structure is four times smaller in magnitude than in the former.

Mn-As bonding in  $\text{CsMn}_4\text{As}_3$  arises largely from interactions between Mn  $4s$ ,  $3d$  and

As  $4p$  orbitals, whereas Mn–Mn bonding comes from Mn  $4s$ ,  $4p$  and Mn  $4s$ ,  $4p$  orbital interactions. It may be noted that Mn  $3d$  along with the  $4s$  and  $4p$  orbitals significantly participate in the chemical bonding with As and thus result in a more delocalized  $3d$  state of Mn compared to our earlier-reported Mn-based intermetallic compounds.<sup>28,29</sup>

**Heat Capacity.** Figure 4 shows the temperature  $T$  variation of the heat capacity  $C_p$  of  $\text{CsMn}_4\text{As}_3$ . The  $C_p$  at  $T = 300$  K is  $213.4$  J/mol K, which is about 7% larger than the expected Dulong-Petit value  $C_V = 3nR = 199.6$  J/mol K, where  $R$  is the molar gas constant and  $n$  is the number of atoms per formula unit which is 8 for  $\text{CsMn}_4\text{As}_3$ . To investigate if this discrepancy originates from a large electronic contribution to the  $C_p$ , we first focus at the low- $T$  data. At low temperatures, in absence of any magnetic contribution or phase transition the  $C_p(T)$  follows

$$C_p = \gamma T + \beta T^3 + \delta T^5, \quad (1)$$

where  $\gamma$  is the electronic Sommerfeld coefficient, and  $\gamma T$  and  $(\beta T^3 + \delta T^5)$  represent the low- $T$  electronic and lattice contributions to the  $C_p$ , respectively. We get a good fit to the data using eq 1 [Inset (a), Fig. 4] and the fitted values of the coefficients are  $\gamma = 5.4(3)$  mJ/mol K<sup>2</sup>,  $\beta = 1.43(3)$  mJ/mol K<sup>4</sup> and  $\delta = 1.05(7) \times 10^{-2}$  mJ/mol K<sup>6</sup>. Using the estimated  $\gamma$ , the electronic contribution to the  $C_p$  at 300 K is calculated as  $1.62$  J/mol K. This is much smaller than the observed enhancement over the Dulong-Petit value, and thus rules out an electronic origin of it. Additionally, our attempt to fit the  $C_p(T)$  of  $\text{CsMn}_4\text{As}_3$  between 1.8 to 300 K using the Debye model<sup>30,31</sup> of acoustic lattice phonons resulted in a poor fit to the data (Fig. 4). These two observations together suggest the presence of a sizable magnetic contribution to  $C_p(T)$  of  $\text{CsMn}_4\text{As}_3$  near room temperature, indicating that  $T_N > 300$  K. A similar observation was made earlier in the case of Fe-doped  $\text{BaMn}_2\text{As}_2$ .<sup>32</sup> High- $T$   $C_p(T)$  data of  $\text{CsMn}_4\text{As}_3$  taken between 290 to 344 K exhibit a jump of about 3 J/mol K at  $T_1 = 324$  K [Inset (b), Fig. 4], which is identified below as a likely magnetic transition temperature where one of the two magnetic moment canting events takes place.

The nonzero value of  $\gamma$  suggests the presence of conduction electron states at  $E_F$  of

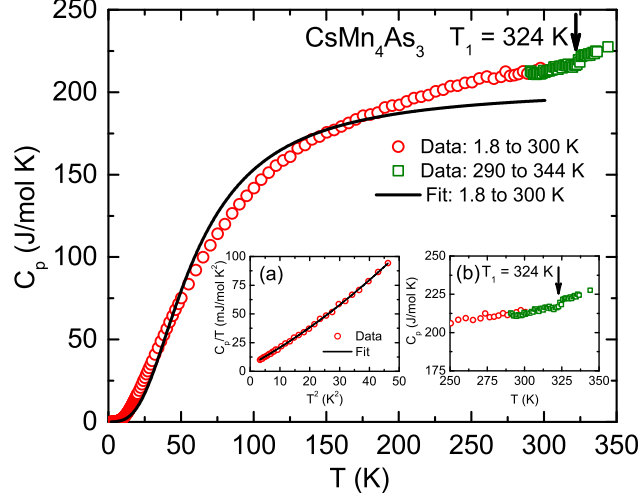


Figure 4: Heat capacity  $C_p$  versus temperature  $T$  for  $\text{CsMn}_4\text{As}_3$ . Open red circle and open green squares are the data taken between 1.8 to 300 K and between 290 to 344 K, respectively. Vertical arrow indicates the transition temperature  $T_1$ . Solid curve is a fit using the Debye model to the data between 1.8 to 300 K. Inset (a): Magnified view of the  $C_p(T)$  data near the transition temperature  $T_1$ . Inset (b): variation of  $C/T$  with  $T$  at low temperature. Solid curve is a fit using the eq 1 described in the text.

$\text{CsMn}_4\text{As}_3$ . The DOS at the  $E_F$   $\mathcal{D}^\gamma(E_F)$  can be estimated from the experimentally estimated  $\gamma$  using

$$\mathcal{D}^\gamma(E_F) \left[ \frac{\text{states}}{\text{eV f.u.}} \right] = \frac{1}{2.359} \gamma \left[ \frac{\text{mJ}}{\text{mol K}^2} \right], \quad (2)$$

where  $\mathcal{D}^\gamma(E_F)$  is for both spin directions. The calculated value of  $\mathcal{D}^\gamma(E_F)$  is 2.3(1) states/eV f.u. for both spin directions. A similar  $\mathcal{D}^\gamma(E_F)$  was observed in the lightly (<5%) hole-doped  $\text{BaMn}_2\text{As}_2$ .<sup>7</sup> The  $\mathcal{D}^\gamma(E_F)$  value is about a factor of two smaller than obtained from the above band structure calculations, suggesting the presence of localization effects in this layered material. From the experimentally determined  $\beta$ , the Debye temperature  $\Theta_D$  of  $\text{CsMn}_4\text{As}_3$  is calculated as  $\Theta_D = (12\pi^4 Rn/5\beta)^{1/3} = 222(2)$  K. The estimated magnetic entropy  $S_{\text{mag}}$  that approaches  $R\ln 6$  at high temperatures [Fig. S4(b), supporting information] suggests the presence of high-spin  $S = 5/2$  state of the  $\text{Mn}^{+2}$  ions in this compound.

**Electrical Resistivity.** The electrical resistivity within the basal plane  $\rho_{ab}$  versus  $T$  data of  $\text{CsMn}_4\text{As}_3$  are shown in the Fig. 5. In agreement with the  $C_p(T)$  data and the band calculations discussed above the  $\rho_{ab}$  has a finite value at the lowest  $T$  of our measurement,

suggesting a non-insulating ground state in this compound. However, the very high value of  $\rho_{ab} \text{ at } 2 \text{ K} = 616.2 \text{ } \Omega \text{ cm}$ , which is several orders of magnitude larger than the resistivities of normal metals, indicates that the material is not a good metal either. While the  $\rho_{ab}$  shows a strong  $T$ -dependence and monotonically decreases to a value of  $1.4 \text{ } \Omega \text{ cm}$  at  $300 \text{ K}$ , it does not show the activated behavior expected in a band semiconductor as evident from the absence of any linear region in  $\ln\rho_{ab}$  versus  $1/T$  plots [Insets (a) and (b), Fig. 5]. These observations collectively suggest that the mechanism of electrical transport in  $\text{CsMn}_4\text{As}_3$  is qualitatively similar to that in the related small band-gap semiconductor  $\text{BaMn}_2\text{As}_2$ , which also shows a non-metallic  $T$ -dependence and a finite sample-dependent  $\rho_{ab}$  at  $T \rightarrow 0$ .<sup>4,6,7</sup> The observed  $T$ -dependence of  $\rho_{ab}$  likely originates from the limited availability of current-carrying  $s$  and  $p$  states at the  $E_F$  of  $\text{CsMn}_4\text{As}_3$ . As evident from the band calculations (Fig. 3) the contribution of the  $s$  and  $p$  states to the  $\mathcal{D}(E_F)$  is only  $\sim 1 \text{ state/eV f.u.}$  for both spin directions, whereas the heavier  $d$  states that may not take part in the conduction contribute  $\sim 4 \text{ states/eV f.u.}$  for both spin directions. From the observations made in the heat capacity and the electrical resistivity measurements as well as from the results of the band calculations it appears that bad-metal type electrical conduction behavior of  $\text{CsMn}_4\text{As}_3$  is an outcome of limited availability of conduction carriers and strong electronic correlations. It appears that similar to the hole-doped  $\text{BaMn}_2\text{As}_2$ , this material can likely be pushed into a metallic ground state by hole/electron doping and/or by the application of external pressure.<sup>33</sup> We have also evaluated the possibility of the variable range hopping<sup>34,35</sup>-type electrical conduction in our material. However, the data do not seem to follow this behavior, especially at the low temperatures (Fig. S5, supporting information).

**Magnetism.** The anisotropic magnetic susceptibilities  $\chi_{ab,c} \equiv M_{ab,c}/H$  of  $\text{CsMn}_4\text{As}_3$  measured in an applied dc magnetic field  $H = 0.1 \text{ T}$  are shown in Fig. 6 (also see Fig. S6, supporting information for corresponding data at  $H = 3.0 \text{ T}$ ). Some noticeable features observed in the  $\chi(T)$  data are the following; (i)  $\chi_c$  decrease monotonically with decreasing  $T$  before showing an upturn at  $T \sim 125 \text{ K}$ , (ii)  $\chi_{ab}$  increases monotonically with decreasing  $T$

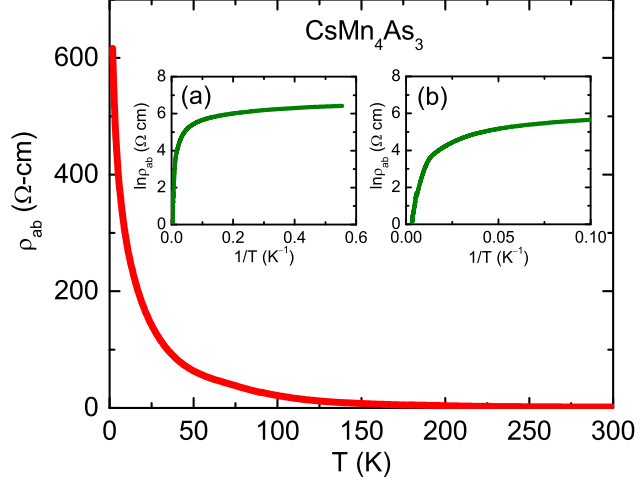


Figure 5: Electrical resistivity  $\rho_{ab}$  measured in the basal  $ab$ -plane versus temperature  $T$  of  $\text{CsMn}_4\text{As}_3$ . Inset (a): resistivity on a logarithmic scale  $\ln\rho_{ab}$  versus  $1/T$ . Inset (b):  $\ln\rho_{ab}$  versus  $1/T$  in a restricted  $1/T$  range.

and exhibits the features that suggest the presence of two magnetic transitions at  $T_1 = 325(5)$  and  $T_2 = 150(5)$  K, respectively.

Since the  $\text{CsMn}_4\text{As}_3$  crystals were grown using the MnAs flux which is a ferromagnet with  $T_c = 313(5)$  K,<sup>36–38</sup> it's natural to consider that the transition observed at 325 K could possibly be an outcome of the inclusion of MnAs impurity in the crystals. However, the absence of this transition in the  $\chi_c(T)$  data taken on the same crystal as well the jump observed in the  $C_p(T)$  at  $T_1$  (Fig. 4) together suggest that this feature is likely a bulk effect intrinsic to the material and is not due to ferromagnetic impurity. Additionally, NiAs-type hexagonal crystal structure and significantly different lattice parameters of MnAs<sup>39</sup> compared to those of  $\text{CsMn}_4\text{As}_3$  reduce the possibility of epitaxial growth of films of the former between the layers or on the surface of the latter, which is required for exhibiting the anisotropic impurity effect as observed in this case. Furthermore, the results obtained on the crystals of similar tetragonal materials grown using the same synthesis process suggest that the inclusion of MnAs impurity produces nearly isotropic effects in the magnetic measurements (Fig. S7, supporting information).

Although neutron diffraction measurements are needed to solve the underlying magnetic structure of this new material, we can still extract some features of the magnetism from

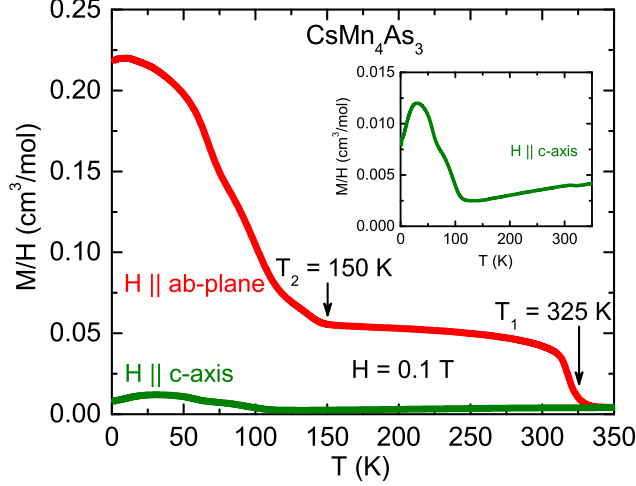


Figure 6: Anisotropic magnetic susceptibilities  $\chi_{ab,c} \equiv M_{ab,c}/H$  versus temperature  $T$  of  $\text{CsMn}_4\text{As}_3$  measured at applied dc magnetic fields of  $H = 0.1$  T. Vertical arrows indicate the two transitions observed in  $\chi_{ab}$  at  $T_1 = 325(5)$  K and  $T_2 = 150(5)$  K, respectively. Inset: expanded plot of the  $\chi_c(T)$ .

the thermodynamic  $\chi(T)$  and  $M(H)$  measurements. Considering the fact that  $\text{CsMn}_4\text{As}_3$  is a small band-gap semiconductor as well as from an analogy with the related  $\text{BaMn}_2\text{As}_2$ , it is likely that the magnetism of this material is of the local moment character where the Mn ion carries the magnetic moment. The  $\chi_c(T)$  of  $\text{CsMn}_4\text{As}_3$  that exhibits a behavior qualitatively similar to the  $\text{BaMn}_2\text{As}_2$ <sup>9,12</sup> suggests an AFM ground state in this material. The  $\chi_c(T)$  data that approach to  $\chi_c \approx 0$  for  $T \rightarrow 0$  (Inset, Fig. 6) when extrapolated from higher temperatures ( $T > 125$  K) suggests that the  $c$ -axis is the magnetic easy axis for the localized Mn-spins which are aligned antiparallel along this direction. The upturn observed in the  $\chi_c(T)$  at 125 K is likely due to a minor misalignment of the crystal with respect to the  $H$ .<sup>9,12</sup> The two transitions observed in  $\chi_{ab}$  at  $T_1$  and  $T_2$  likely arise from canting of the localized Mn-spins aligned along the tetragonal  $c$ -axis towards the  $ab$ -plane. The canting of the moment toward the  $ab$ -plane likely arises from a lattice distortion giving rise to an antisymmetric Dzyaloshinskii-Moriya interaction<sup>40</sup> and similar to the magnetic transitions in  $\text{CaFe}_4\text{As}_3$ ,<sup>41,42</sup> it could also involve a commensurate  $\leftrightarrow$  incommensurate transition.

As evident from the isothermal magnetization  $M_{ab}$  versus  $H$  measurements, these two successive canting events lead to small FM moments of  $\mu_{1ab} \approx 0.01 \mu_B$  and  $\mu_{2ab} \approx 0.045 \mu_B/\text{Mn}$

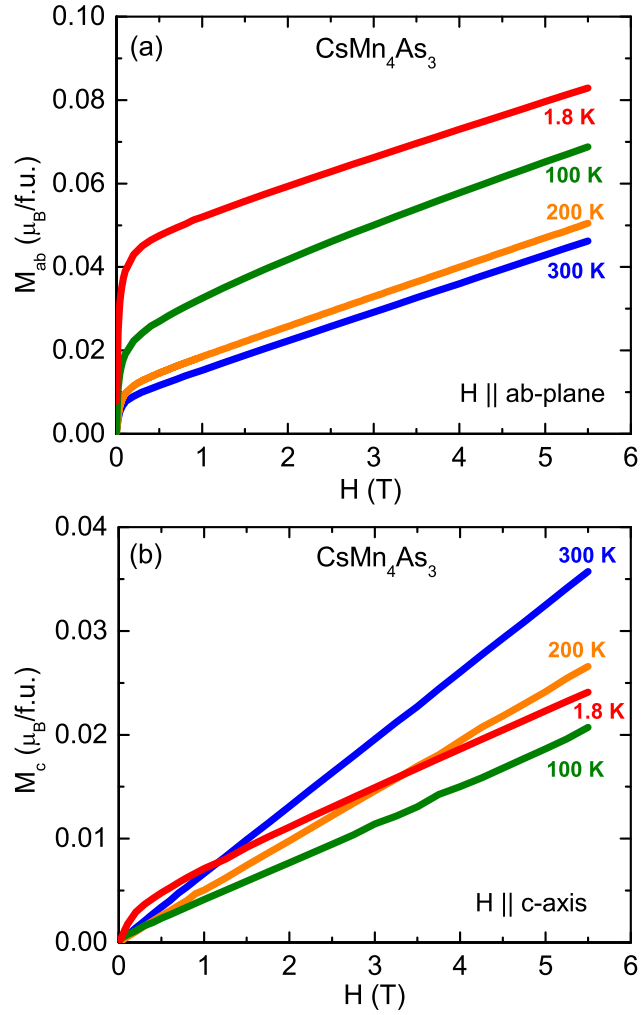


Figure 7: Isothermal magnetization  $M$  versus applied magnetic field  $H$  data of  $\text{CsMn}_4\text{As}_3$  taken at four temperatures between 1.8 and 300 K for  $H$  along the (a)  $ab$ -plane and (b)  $c$ -axis.

at 300 and 1.8 K, respectively [Fig. 7(a)]. If we assume that the moment associated with the localized Mn-spins in  $\text{CsMn}_4\text{As}_3$  are of the similar size ( $\mu_{\text{Mn}} \approx 4 \mu_{\text{B}}$ ) of that in  $\text{BaMn}_2\text{As}_2$  as indicated by the above band structure calculations, then the canting angles  $\theta_1$  and  $\theta_2$  associated with the canting events occurring at  $T_1$  and  $T_2$ , respectively, can be calculated as

$$\mu_{\text{Mn}} \cos(90^\circ - \theta_n) = \mu_{nab}/2. \quad (3)$$

Using eq 3, we estimate the canting angles as  $\theta_1 = 0.07^\circ$  and  $\theta_2 = 0.32^\circ$ .

Variations of  $M_c$  with  $H$  are shown for four temperatures in Fig. 7(b). At high temperatures ( $T > 100$  K), following a behavior expected from an AFM material the  $M_c$  varies linearly with  $H$ . However, for  $T \leq 100$  K, the  $M_c(H)$  data start deviating from the linear  $H$  dependence and develop a very small ordered moment  $\mu_c \approx 0.004 \mu_{\text{B}}$  at 1.8 K. As discussed before, the observed small ordered moment likely originates from a  $\approx 4.8^\circ$  misalignment of the tetragonal  $c$ -axis with  $\mathbf{H}$ .

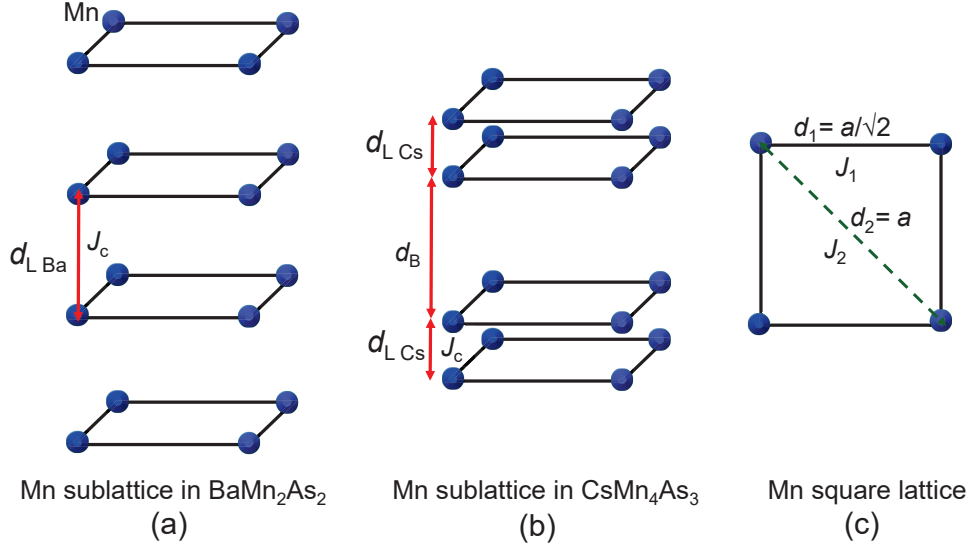


Figure 8: Representations of the Mn sublattices in (a)  $\text{BaMn}_2\text{As}_2$  and (b)  $\text{CsMn}_4\text{As}_3$ . The inter-layer distances  $d_{\text{L Ba}}$ ,  $d_{\text{L Cs}}$  and  $d_{\text{B}}$  are shown on a proportional scale. (c) The top view of the Mn square lattice. Intralayer ( $J_1$  and  $J_2$ ) and interlayer ( $J_c$ ) magnetic exchange interactions are indicated in each panel.

Although, apart from the canting of the moment toward the  $ab$ -plane, the magnetic

characteristics of  $\text{CsMn}_4\text{As}_3$  appear qualitatively similar to  $\text{BaMn}_2\text{As}_2$  the Mn sublattice is very different in both the compounds. While in  $\text{BaMn}_2\text{As}_2$  the layers of Mn square lattice are equidistantly placed along the crystallographic  $c$ -direction with the interlayer distance  $d_{\text{L Ba}} = c(1 - 2z_{\text{Mn}}) = 6.7341(4) \text{ \AA}$ , the Mn-atoms form bilayers in  $\text{CsMn}_4\text{As}_3$  (Fig. 8). Within a bilayer the interlayer distance is  $d_{\text{L Cs}} = c(1 - 2z_{\text{Mn}}) = 3.1661(6) \text{ \AA}$ , which is only about 40% of the distance  $d_{\text{B}} = 2cz_{\text{Mn}} = 7.290(6) \text{ \AA}$  of the next-nearest layer that belongs to the adjacent bilayer. In fact, the  $d_{\text{L Cs}}$  in  $\text{CsMn}_4\text{As}_3$  is nearly equal to the intralayer nearest neighbor (NN) distance  $d_1 = a/\sqrt{2} = 3.0322(2) \text{ \AA}$  and 26% smaller than the intralayer next nearest neighbor (NNN) distance  $d_2 = a = 4.2882(2) \text{ \AA}$  (Fig. 8). These significant differences between the Mn sublattices of  $\text{CsMn}_4\text{As}_3$  and well-known  $\text{BaM}_2\text{As}_2$  ( $M$ : Cr, Mn, Fe, Co, Ni, Cu, Ru, Rh and Pd) compounds are bound to change the strengths of the exchange interactions as well as their interplay in the former compared to the latter within the  $J_1$ - $J_2$ - $J_c$  model.<sup>43</sup> Thus, this new material lays the foundation of a new playground where systematic investigations in the search of exciting electronic and/or magnetic properties can be performed by doping and pressure studies.

## Summary and Conclusions

We have discovered a new layered tetragonal ternary compound  $\text{CsMn}_4\text{As}_3$  (structure type:  $\text{KCu}_4\text{S}_3$ , space group:  $P4/mmm$ , No. 123 and  $Z = 2$ ). Our physical property measurements show that similar to the related  $\text{ThCr}_2\text{Si}_2$ -type tetragonal  $\text{BaMn}_2\text{As}_2$  this compound is a small band-gap semiconductor, thus the underlying magnetism very likely originates from localized Mn spins. Our magnetic measurements suggest that this compound has an AFM ground state with  $T_{\text{N}} > 300 \text{ K}$  and the magnetic easy axis is likely along the crystallographic  $c$ -axis. The magnetic susceptibility and magnetization data within the basal  $ab$ -plane show the signature of two magnetic moment canting events at  $T_1 = 325(5)$  and  $T_2 = 150(5) \text{ K}$  with a low- $T$  canting angles  $\theta_1 \approx 0.1^\circ$  and  $\theta_2 \approx 0.3^\circ$ , respectively. While the transition at

$T_2$  almost certainly is intrinsic to the material, further work is needed to categorically resolve whether or not the transition at  $T_1$  is intrinsic or is an artifact of epitaxially grown FM impurities between the layers or on the surface of  $\text{CsMn}_4\text{As}_3$ . Although the magnetic properties of  $\text{CsMn}_4\text{As}_3$  appear qualitatively similar to the well-studied  $\text{BaMn}_2\text{As}_2$ , the underlying Mn sublattice is very different. While in  $\text{BaMn}_2\text{As}_2$  the layers of the Mn square lattice are equidistant along the  $c$ -axis with interlayer distance  $d_{\text{L Ba}} = 6.7341(4) \text{ \AA}$ , the Mn ions form a bilayer in  $\text{CsMn}_4\text{As}_3$  with the interlayer distance within the bilayer  $d_{\text{L Cs}} = 3.1661(6) \text{ \AA}$  and next-nearest interlayer distance between the adjacent bilayers  $d_{\text{B}} = 7.290(6) \text{ \AA}$ . This modification leads into a situation where  $d_{\text{L Cs}}$  is approximately equal to the NN distance  $d_1$  as well as smaller than the NNN distance  $d_2$  within the Mn square lattice. These variations in the underlying Mn sublattice likely alter the energy balance between the exchange interactions within the  $J_1$ - $J_2$ - $J_c$  model compared to those in  $\text{BaMn}_2\text{As}_2$ .

This new 143-type addition to the family of layered tetragonal compounds related to Fe-based superconductors brings exciting opportunities to look for interesting magnetic as well as plausible superconducting ground states. While neutron diffraction and scattering experiments are needed to solve the magnetic structure as well as to determine the estimates of the strengths of the exchange interactions, doping and pressure studies with the aim of discovering new superconductors or other interesting ground states might be a fruitful endeavor.

**Supporting Information.** Figures showing the powder x-ray diffraction data and their refinement, nearest-neighbor environments around Cs, Mn, As1 and As2 atoms in  $\text{CsMn}_4\text{As}_3$ , spin alignment in the A-type antiferromagnetic model used for the band structure calculations, estimation of magnetic entropy, evaluation of electrical resistivity data in the context of variable range hopping model, magnetic susceptibility versus temperature data of  $\text{CsMn}_4\text{As}_3$  measured at  $H = 3 : 0 \text{ T}$ , effect of MnAs impurity on the susceptibility of the related compound  $\text{Ba}_{0.6}\text{K}_{0.4}\text{Mn}_2\text{As}_2$ , table containing the anisotropic displacement parameters of Cs, Mn, As1 and As2 atoms estimated from single-crystal x-ray diffraction data of  $\text{CsMn}_4\text{As}_3$ ,

and a crystallographic information file.

## Acknowledgement

The research at Ames Laboratory was supported by the U.S. Department of Energy, Office of Basic Energy Sciences, Division of Materials Sciences and Engineering. Ames Laboratory is operated for the U.S. Department of Energy by Iowa State University under Contract No. DE-AC02-07CH11358.

## References

- (1) Johnston, D. C. In *Handbook of Magnetic Materials*; Buschow, K. H. J., Ed.; Elsevier: Amsterdam, Neatherlands, 1997; Vol. 10; Chapter 1, pp 1–237.
- (2) Johnston, D. C. The puzzle of high temperature superconductivity in layered iron pnictides and chalcogenides. *Adv. Phys.* **2010**, *59*, 803–1061.
- (3) Anand, V. K.; Kim, H.; Tanatar, M. A.; Prozorov, R.; Johnston, D. C. Superconducting and normal-state properties of  $APd_2As_2$  ( $A = Ca, Sr, Ba$ ) single crystals. *Phys. Rev. B* **2013**, *87*, 224510.
- (4) Singh, Y.; Ellern, A.; Johnston, D. C. Magnetic, transport, and thermal properties of single crystals of the layered arsenide  $BaMn_2As_2$ . *Phys. Rev. B* **2009**, *79*, 094519.
- (5) Singh, Y.; Green, M. A.; Huang, Q.; Kreyssig, A.; McQueeney, R. J.; Johnston, D. C.; Goldman, A. I. Magnetic order in  $BaMn_2As_2$  from neutron diffraction measurements. *Phys. Rev. B* **2009**, *80*, 100403.
- (6) An, J.; Sefat, A. S.; Singh, D. J.; Du, M.-H. Electronic structure and magnetism in  $BaMn_2As_2$  and  $BaMn_2Sb_2$ . *Phys. Rev. B* **2009**, *79*, 075120.

- (7) Pandey, A.; Dhaka, R. S.; Lamsal, J.; Lee, Y.; Anand, V. K.; Kreyssig, A.; Heitmann, T. W.; McQueeney, R. J.; Goldman, A. I.; Harmon, B. N.; Kaminski, A.; Johnston, D. C.  $\text{Ba}_{1-x}\text{K}_x\text{Mn}_2\text{As}_2$ : An Antiferromagnetic Local-Moment Metal. *Phys. Rev. Lett.* **2012**, *108*, 087005.
- (8) Lamsal, J.; Tucker, G. S.; Heitmann, T. W.; Kreyssig, A.; Jesche, A.; Pandey, A.; Tian, W.; McQueeney, R. J.; Johnston, D. C.; Goldman, A. I. Persistence of local-moment antiferromagnetic order in  $\text{Ba}_{1-x}\text{K}_x\text{Mn}_2\text{As}_2$ . *Phys. Rev. B* **2013**, *87*, 144418.
- (9) Pandey, A.; Ueland, B. G.; Yeninas, S.; Kreyssig, A.; Sapkota, A.; Zhao, Y.; Helton, J. S.; Lynn, J. W.; McQueeney, R. J.; Furukawa, Y.; Goldman, A. I.; Johnston, D. C. Coexistence of Half-Metallic Itinerant Ferromagnetism with Local-Moment Antiferromagnetism in  $\text{Ba}_{0.60}\text{K}_{0.40}\text{Mn}_2\text{As}_2$ . *Phys. Rev. Lett.* **2013**, *111*, 047001.
- (10) Yeninas, S.; Pandey, A.; Ogloblichev, V.; Mikhalev, K.; Johnston, D. C.; Furukawa, Y. Metal-insulator transition in antiferromagnetic  $\text{Ba}_{1-x}\text{K}_x\text{Mn}_2\text{As}_2$  ( $0 \leq x \leq 0.4$ ) single crystals studied by  $^{55}\text{Mn}$  and  $^{75}\text{As}$  NMR. *Phys. Rev. B* **2013**, *88*, 241111.
- (11) Ueland, B. G.; Pandey, A.; Lee, Y.; Sapkota, A.; Choi, Y.; Haskel, D.; Rosenberg, R. A.; Lang, J. C.; Harmon, B. N.; Johnston, D. C.; Kreyssig, A.; Goldman, A. I. Itinerant Ferromagnetism in the As 4*p* Conduction Band of  $\text{Ba}_{0.6}\text{K}_{0.4}\text{Mn}_2\text{As}_2$  Identified by X-Ray Magnetic Circular Dichroism. *Phys. Rev. Lett.* **2015**, *114*, 217001.
- (12) Pandey, A.; Johnston, D. C.  $\text{Ba}_{0.4}\text{Rb}_{0.6}\text{Mn}_2\text{As}_2$ : A prototype half-metallic ferromagnet. *Phys. Rev. B* **2015**, *92*, 174401.
- (13) Ramazanoglu, M.; Sapkota, A.; Pandey, A.; Lamsal, J.; Abernathy, D. L.; Niedziela, J. L.; Stone, M. B.; Kreyssig, A.; Goldman, A. I.; Johnston, D. C.; McQueeney, R. J. Robust antiferromagnetic spin waves across the metal-insulator transition in hole-doped  $\text{BaMn}_2\text{As}_2$ . *Phys. Rev. B* **2017**, *95*, 224401.

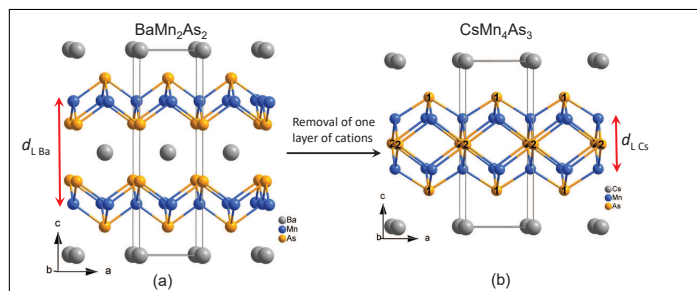
- (14) Rüdorff, W.; Schwarz, H. G.; Walter, M. Alkalithio- und -selenoverbindungen der Übergangselemente. III. Strukturuntersuchungen an Alkalithiocupraten. *Z. Anorg. Allg. Chem.* **1952**, *269*, 141–152.
- (15) Brown, D. B.; Zubietta, J. A.; Vella, P. A.; Wroblewski, J. T.; Watt, T.; Hatfield, W. E.; Day, P. Solid-state structure and electronic properties of a mixed-valence two-dimensional metal, potassium copper sulfide ( $\text{KCu}_4\text{S}_3$ ). *Inorg. Chem.* **1980**, *19*, 1945–1950.
- (16) He, H.; Tyson, C.; Bobev, S. Eight-Coordinated Arsenic in the Zintl Phases  $\text{RCd}_4\text{As}_3$  and  $\text{RbZn}_4\text{As}_3$ : Synthesis and Structural Characterization. *Inorg. Chem.* **2011**, *50*, 8375–8383, PMID: 21812395.
- (17) Rodríguez-Carvajal, J. Recent advances in magnetic structure determination by neutron powder diffraction. *Physica B* **1993**, *192*, 55 – 69.
- (18) *SMART*; Bruker AXS, Inc.: Madison, USA, 1996.
- (19) Blessing, R. H. An empirical correction for absorption anisotropy. *Acta Crystallogr. A* **1995**, *51*, 33–38.
- (20) *SHELXTL*; Bruker AXS, Inc.: Madison, USA, 2000.
- (21) Krier, G.; Jepsen, O.; Burkhardt, A.; Andersen, O. K. TBLMTO-ASA Program, version 4.7. Max-Planck-Institut für Festkörperforschung: Stuttgart, Germany, 1995.
- (22) Koelling, D. D.; Harmon, B. N. A technique for relativistic spin-polarised calculations. *J. Phys. C* **1977**, *10*, 3107.
- (23) Jepsen, O.; Andersen, O. K. Calculated electronic structure of the sandwiched metals  $\text{LaI}_2$  and  $\text{CeI}_2$ : Application of new LMTO techniques. *Z. Phys. B* **1995**, *97*, 35–47.

- (24) Dronskowski, R.; Bloechl, P. E. Crystal orbital Hamilton populations (COHP): energy-resolved visualization of chemical bonding in solids based on density-functional calculations. *J. Phys. Chem* **1993**, *97*, 8617–8624.
- (25) Samal, S. L.; Gulo, F.; Corbett, J. D. Cluster Chemistry in Electron-Poor Ae-Pt-Cd Systems (Ae = Ca, Sr, Ba): (Sr, Ba)Pt<sub>2</sub>Cd<sub>4</sub>, Ca<sub>6</sub>Pt<sub>8</sub>Cd<sub>16</sub>, and Its Known Antitype Er<sub>6</sub>Pd<sub>16</sub>Sb<sub>8</sub>. *Inorg. Chem.* **2013**, *52*, 2697–2704, PMID: 23418724.
- (26) Todorov, I.; Chung, D. Y.; Malliakas, C. D.; Li, Q.; Bakas, T.; Douvalis, A.; Tri-marchi, G.; Gray, K.; Mitchell, J. F.; Freeman, A. J.; Kanatzidis, M. G. CaFe<sub>4</sub>As<sub>3</sub>: A Metallic Iron Arsenide with Anisotropic Magnetic and Charge-Transport Properties. *J. Am. Chem. Soc.* **2009**, *131*, 5405–5407, PMID: 19334680.
- (27) Samal, S. L.; Corbett, J. D. Relativistic Effects and Gold Site Distributions: Synthesis, Structure, and Bonding in a Polar Intermetallic Nd<sub>6</sub>Cd<sub>16</sub>Au<sub>7</sub>. *Inorg. Chem.* **2011**, *50*, 7033–7039, PMID: 21728282.
- (28) Samal, S. L.; Pandey, A.; Johnston, D. C.; Corbett, J. D. Y<sub>3</sub>MnAu<sub>5</sub>: Three Distinctive d-Metal Functions in an Intergrown Cluster Phase. *J. Am. Chem. Soc.* **2013**, *135*, 910–917, PMID: 23259905.
- (29) Samal, S. L.; Pandey, A.; Johnston, D. C.; Corbett, J. D.; Miller, G. J. Taking Advantage of Gold’s Electronegativity in R<sub>3</sub>Mn<sub>3-x</sub>Au<sub>10+x</sub> (R = Gd or Y; 0.2 ≤ x ≤ 1). *Chem. Mater.* **2014**, *26*, 3209–3218.
- (30) Gopal, E. S. R. *Specific Heat at Low Temperatures*; Plenum: New York, USA, 1966.
- (31) Goetsch, R. J.; Anand, V. K.; Pandey, A.; Johnston, D. C. Structural, thermal, magnetic, and electronic transport properties of the LaNi<sub>2</sub>(Ge<sub>1-x</sub>P<sub>x</sub>)<sub>2</sub> system. *Phys. Rev. B* **2012**, *85*, 054517.

- (32) Pandey, A.; Anand, V. K.; Johnston, D. C. Large miscibility gap in the  $\text{Ba}(\text{Mn}_x\text{Fe}_{1-x})_2\text{As}_2$  system. *Phys. Rev. B* **2011**, *84*, 014405.
- (33) Satya, A. T.; Mani, A.; Arulraj, A.; Shekar, N. V. C.; Vinod, K.; Sundar, C. S.; Bharathi, A. Pressure-induced metallization of  $\text{BaMn}_2\text{As}_2$ . *Phys. Rev. B* **2011**, *84*, 180515.
- (34) Mott, N. F. Conduction in non-crystalline materials. *The Philosophical Magazine: A Journal of Theoretical Experimental and Applied Physics* **1969**, *19*, 835–852.
- (35) Shklovskii, B. I.; Efros, A. L. *Electronic Properties of Doped Semiconductors*; Springer-Verlag: Berlin Heidelberg, 1984.
- (36) Bean, C. P.; Rodbell, D. S. Magnetic Disorder as a First-Order Phase Transformation. *Phys. Rev.* **1962**, *126*, 104–115.
- (37) Haneda, S.; Kazama, N.; Yamaguchi, Y.; Watanabe, H. Electronic State of High Spin MnAs. *J. Phys. Soc. Jpn.* **1977**, *42*, 1201–1211.
- (38) Maki, K.; Kaneko, T.; Hiroyoshi, H.; Kamigaki, K. Crystalline and magnetic properties of MnAs under pressure. *J. Magn. Magn. Mater.* **1998**, *177*, 1361 – 1362.
- (39) Wilson, R. H.; Kasper, J. S. The crystal structure of MnAs above 40°C. *Acta Crystallogr.* **1964**, *17*, 95–101.
- (40) Glasbrenner, J. K.; Mazin, I. I. First-principles evidence of Mn moment canting in hole-doped  $\text{Ba}_{1-2x}\text{K}_{2x}\text{Mn}_2\text{As}_2$ . *Phys. Rev. B* **2014**, *89*, 060403.
- (41) Zhao, L. L.; Yi, T.; Fettinger, J. C.; Kauzlarich, S. M.; Morosan, E. Fermi-liquid state and enhanced electron correlations in the iron pnictide  $\text{CaFe}_4\text{As}_3$ . *Phys. Rev. B* **2009**, *80*, 020404.

- (42) Nambu, Y.; Zhao, L. L.; Morosan, E.; Kim, K.; Kotliar, G.; Zajdel, P.; Green, M. A.; Ratcliff, W.; Rodriguez-Rivera, J. A.; Broholm, C. Incommensurate Magnetism in FeAs Strips: Neutron Scattering from  $\text{CaFe}_4\text{As}_3$ . *Phys. Rev. Lett.* **2011**, *106*, 037201.
- (43) Johnston, D. C.; McQueeney, R. J.; Lake, B.; Honecker, A.; Zhitomirsky, M. E.; Nath, R.; Furukawa, Y.; Antropov, V. P.; Singh, Y. Magnetic exchange interactions in  $\text{BaMn}_2\text{As}_2$ : A case study of the  $J_1$ - $J_2$ - $J_c$  Heisenberg model. *Phys. Rev. B* **2011**, *84*, 094445.

## Graphical TOC Entry



**Synopsis:** Two layers of  $[\text{Mn}_2\text{As}_2]^{2-}$  in  $\text{BaMn}_2\text{As}_2$  are condensed into a single  $[\text{Mn}_4\text{As}_3]$  layer in the new compound  $\text{CsMn}_4\text{As}_3$  by removal of the intermediate layer of the cation as a consequence of the weak Cs-As bonding.